High-order harmonic generation in a driven two-level atom: Periodic level crossings and three-step processes

C. Figueira de Morisson Faria
Max Born Institut für nichtlineare Optik und Kurzzeitspektroskopie, Max Born Strasse 2A, D-12489 Berlin, Germany

I. Rotter
Max Planck Institut für Physik komplexer Systeme, Nöthnitzer Strasse 38, D-01187 Dresden, Germany

(Received 20 December 2001; published 15 July 2002)

We investigate high-order harmonic generation in closed systems using the two-level atom as a simplified model. By means of a windowed Fourier transform of the time-dependent dipole acceleration, we extract the main contributions to this process within a cycle of the driving field. We show that the patterns obtained can be understood by establishing a parallel between the two-level atom and the three-step model. In both models, high-order harmonic generation is a consequence of a three-step process, which involves either the continuum and the ground state, or the adiabatic states of the two-level Hamiltonian. The knowledge of this physical mechanism allows us to manipulate the adiabatic states, and consequently the harmonic spectra, by means of a bichromatic driving field. Furthermore, using scaling laws, we establish sharp criteria for the invariance of the physical quantities involved. Consequently, our results can be extended to a broader parameter range, as, for instance, those characteristic of solid-state systems in strong fields.

DOI: 10.1103/PhysRevA.66.013402 PACS number(s): 42.50.Hz, 32.80.Rm, 32.80.Qk, 42.65.Ky

I. INTRODUCTION

The generation of high-order harmonics of a strong laser field ($I \sim 10^{14}$ W/cm^2) in gaseous samples, where coherent light in the extreme ultraviolet regime is obtained from infrared input radiation, originated a breakthrough in nonlinear optics. In these systems, composed by atoms or small molecules, high-order harmonic generation (H.H.G.) is a well-understood issue [1] . These highly nonlinear spectra exhibit very particular features: a frequency region with harmonics of roughly the same intensities, the ''plateau,'' and a sharp decrease in the harmonic yield at the plateau's high-energy end, the ''cutoff.'' Since the early 1990s, not only these features have been investigated, but also the HHG time profile [2,3], physical mechanisms [4,5], and the propagation of the harmonic radiation in gaseous media [6]. These studies culminated with countless proposals of how to control high harmonics, as diverse as, for instance, polychromatic [7–9] or static [10] fields, ultrashort pulses [11], or additional potentials [12], many of them having even been realized experimentally [13].

One of the first models proposed to describe high-order harmonic generation in atoms or diatomic molecules was a two-level atom [4]. Within this framework, a particularly important paper is [14]. Therein, it is shown that these harmonics are a consequence of the population transfer between the field-dependent states obtained from the diagonalization of the two-level Hamiltonian. This physical mechanism has not been investigated in detail, and there is a very simple reason for this apparent lack of interest: it turned out that an at first sight completely different physical picture is far more successful in explaining high-order harmonic generation for these systems. This picture, known as ''the three-step model,'' portraits high-order harmonic generation as a process in which an electron leaves an atom at an instant t_0 (the first step), propagates in the continuum being accelerated by the field (the second step), and recombines with the ground state of its parent ion [5] at a later time t_1, emitting a high-order harmonic photon (the third step). This model has shown that the interplay between a bound state and the continuum, which is not present in a two-level atom, is essential for a correct physical description of high-order harmonic generation. Thus the three-step model has established itself as the paradigm for describing this phenomenon (see, e.g., [15] for a comparison of both models).

Until very recently, only gaseous systems were believed to be possible high-order harmonic sources, due to the high intensities involved. However, nowadays, this picture has changed. With the advent of short pulses, there are solid-state materials which can survive the necessary intensity regime, namely $10^{12}-10^{14}$ W/cm^2 [16]. This has led to theoretical studies on high-order harmonic generation in materials such as thin crystals [17] or carbon nanotubes [18]. Another example of a new and unexpected effect is, for instance, carrier-wave Rabi flopping, which has been recently measured experimentally [19].

Furthermore, apart from this entirely new parameter range, even for considerably lower driving-field intensities, as, for instance, $I \sim 10^6$ W/cm^2, one may in principle extend the frequency of far-infrared radiation ($\omega \sim 1$ GHz) in up to two orders of magnitude by using adequate materials. For instance, for GaAs/Al_xGa_{1-x}As wells intersubband transitions of $\omega_0 \sim 1$ THz may serve this purpose [20]. Apart from these solid-state materials, HHG involving larger molecules is becoming a problem of interest [21,22].

For these complex systems, it is not entirely clear whether bound-to-continuum transitions still yield the most adequate description of high-order harmonic generation. In fact, recent studies have shown that, for aromatic molecules, transitions involving solely bound states are far more important for high-order harmonic generation than the interplay between the ground state and the continuum [22]. Thus theoretical

approaches in which the continuum is not taken into account may be possibly used to describe this phenomenon in systems as, for instance, quantum wells [20,23–26]. Furthermore, descriptions of nonlinear optical processes in solids are widely based on the Hartree-Fock semiconductor Bloch equations. Under special conditions, such as low doping density, equal effective masses in both subbands involved, parallel subbands, and not too wide wells, these equations are formally identical to those describing the evolution of a two-level atom. Otherwise, collective effects must be taken into account and this analogy is lost [20,24–26].

A common characteristic of all the above-stated systems is their intrincated internal structure, with the presence, as the external parameters are varied, of several level crossings. In particular concerning HHG, the periodic level crossings caused by the temporal dependence of the laser field are very important [14]. Thus, in order to control the harmonic spectra also in this context, one needs to understand the interplay between the population transfer at these crossings and high-order harmonic generation.

Even in the simplest case for which these level crossings occur, namely a two-level atom, it is only clear that most of the population transfer between the field-dressed states takes place at the level crossings. However, this does not necessarily mean that the population transfers, within a field cycle, which contribute to the generation of a particular group of harmonics, occur at the level-crossing times. Unanswered questions in this framework concern not only these times, but also how they depend on the external-field parameters, such as its intensity and frequency, and how one can use this information to control the emission spectra of a ''closed,'' nonionizing system. Another interesting issue concerns the existence of a one-to-one correspondence between the three-step model and the two-level atom. This was proposed in [14] due to the different time scales involved in the process, and in [20] due to a formally identical expression describing population transfers in both models. In these references, however, there is no proof that this correspondence really holds.

The answer to these questions is the main objective of this work. The paper is organized as follows: in Sec. II we briefly discuss the theoretical background for the studies performed in this paper. In the following sections we present our results. In Sec. III, we concentrate on a detailed analysis of the population transfers and the time profile of harmonic generation for a monochromatic field. Subsequently (Sec. IV), we provide concrete examples of how an additional driving field may alter the periodic level crossings, and consequently the harmonic emission of a closed system. Furthermore, we address the scaling behavior of the physical quantities involved (Sec. V), establishing sharp criteria for their invariance. Finally, in Sec. VI we close the paper with some concluding remarks.

II. BACKGROUND

A. Two-level atom

The simplest case for which level crossings occur, and a widely used approximation for describing physical systems, is a two-level atom [27]. Within this picture, the time-dependent wave function is given by

$$|\psi(t)\rangle = C_0(t)|\phi_0\rangle + C_1(t)|\phi_1\rangle, \tag{1}$$

where $C_n(t) = \langle \phi_n | \psi(t) \rangle$ denotes the overlap of the total wave function with the nth state of an arbitrary basis. The evolution of the system is described by the time-dependent Schrödinger equation,

$$i\frac{d}{dt}\begin{pmatrix} C_0(t) \\ C_1(t) \end{pmatrix} = H\begin{pmatrix} C_0(t) \\ C_1(t) \end{pmatrix}, \tag{2}$$

where H is the Hamiltonian matrix, which, in our case, describes an atom in an external laser field. We use atomic units throughout. The basis states $|\phi_n\rangle$ are chosen according to the problem at hand. We are particularly interested in a basis which yields sharp, well-separated level crossings in the strong-field regime.

A widely used basis are the field-free-states, also known as the ''diabatic basis.'' In this case, the Hamiltonian is given by

$$H^D = \begin{pmatrix} -\omega_{10}/2 & x_{10}E(t) \\ x_{10}E(t) & \omega_{10}/2 \end{pmatrix}, \tag{3}$$

where ω_{10} is the transition frequency between the field-free bound states, $E(t) = E_0 f(t)$ is the external field, and x_{10} the dipole matrix element $\langle \phi_0^D | \hat{x} | \phi_1^D \rangle$, where $|\phi_n^D\rangle$ denotes the field-free, ''diabatic'' basis states. This basis is very convenient for studying level crossings in the low-intensity laser field regime. For strong laser fields, however, the field-free states are too strongly mixed, such that a more appropriate basis is needed. Such a basis, which will be called by us ''exchanged basis,'' is obtained applying the unitary transformation

$$U_{D\to E} = \frac{1}{\sqrt{2}}\begin{pmatrix} 1 & 1 \\ -1 & 1 \end{pmatrix} \tag{4}$$

onto the diabatic basis. The transformation (4) was used in [14] to interchange the diagonal and the nondiagonal terms of the Hamiltonian (3). In this case, the exchanged-basis energies $\varepsilon_{\pm}^{E} = \pm x_{10}E(t)$ cross, and the coupling which causes the crossing is effectively given by $\omega_{10}/2$. The crossings occur within a time interval $t_0 - t_c < t < t_0 + t_c$, where t_c is the time for which the off-diagonal and diagonal terms of the Hamiltonian become equal and t_0 is the time for which the field vanishes. For strong enough fields, the times over which the crossings take place are much smaller than the period of the driving field. Thus, to first approximation, one may assume that the crossings take place instantaneously at t_0. In the following we call t_0 ''crossing times.''

Another important set of basis states are these which diagonalize H. This basis is the so-called ''adiabatic basis,'' in the sense that the states ''follow'' the field, and is obtained by means of the unitary transformation

$$U_{D\to A}=\begin{pmatrix}\cos\chi & \sin\chi\\ -\sin\chi & \cos\chi\end{pmatrix}, \tag{5}$$

with $\chi=-1/2\arctan[2x_{10}E(t)/\omega_{10}]$. This gives

$$H^A=U_{D\to A}HU^T_{D\to A}=\begin{pmatrix}\varepsilon^A_- & 0\\ 0 & \varepsilon^A_+\end{pmatrix}, \tag{6}$$

where the field-dressed energies are given by

$$\varepsilon^A_\pm=\pm\frac{1}{2}\sqrt{\omega^2_{10}+[2x_{10}E(t)]^2}. \tag{7}$$

Applying $U_{D\to A}$ to the diabatic basis states, one obtains the field-dressed, ''adiabatic'' states

$$|\phi^A_0(t)\rangle=\cos\chi|\phi^D_0\rangle+\sin\chi|\phi^D_1\rangle \tag{8}$$

and

$$|\phi^A_1(t)\rangle=-\sin\chi|\phi^D_0\rangle+\cos\chi|\phi^D_1\rangle, \tag{9}$$

whose energies are, respectively, ε^A_- and ε^A_+ [28]. In order to compute the harmonic spectra, one needs the Fourier transform of the time-dependent dipole. This quantity is given, in its length and acceleration form, by

$$x=x_{10}[g(t)\cos 2\chi+h(t)\sin 2\chi] \tag{10}$$

and

$$\ddot{x}=-\omega^2_{10}x+2\omega_{10}x^2_{10}E(t)[h(t)\cos 2\chi-g(t)\sin 2\chi], \tag{11}$$

respectively, with $g(t)=C^{*A}_0(t)C^A_1(t)+C^{*A}_1(t)C^A_0(t)$ and $h(t)=|C^A_0(t)|^2-|C^A_1(t)|^2$, where $C^A_n(t)=\langle\phi^A_n(t)|\psi(t)\rangle$ denotes the projection of the wave function $|\psi(t)\rangle$ onto an adiabatic state. The equations above are the superposition of two distinct terms, namely the crossed terms and the population difference between the adiabatic states. Since the population difference $h(t)$ roughly ''follows'' the field, it contributes mainly to the generation of low harmonics, whereas $g(t)$ is expected to be responsible for the high harmonics. This has been confirmed by numerical studies (not shown).

An interesting feature is that, in the extreme limit $E_0\to\infty$, the transformation (5) formally corresponds to Eq. (4) and the dipole length (10) becomes proportional to the population difference between the adiabatic states. However, one should keep in mind that, only in this limit, the states obtained using Eq. (4) on the field-free states and the adiabatic states are formally equivalent. In general, this is not the case.

In the subsequent sections, we work mainly in the adiabatic basis, and refer to crossings of the exchanged-basis energies. For the adiabatic energies, there are avoided crossings. The results discussed in this paper have been obtained from the numerical solution of Eq. (2) in the adiabatic basis, by means of a fourth-order Runge-Kutta method. Unless stated otherwise, the driving field is turned on instantaneously.

B. Windowed Fourier transform

For both open and closed systems, high-order harmonic generation is always related to abrupt population transfers. Depending on the group of harmonics, they occur at particular times, which give the main contributions to high-order harmonic generation within a field cycle. For an atom in a strong laser field, for instance, these times are well-known and correspond to the return times t_1 of an electron which left an atom at a previous time t_0. For a closed system, the times t_0 correspond to the level-crossing times and the times t_1 are still an open question to some extent. A very useful method to extract these latter times from the time-dependent dipole is performing a Fourier transform with a temporally restricted window function. For an arbitrary function $f(t')$, this transform is

$$\mathcal{F}(t,\Omega,\sigma)=\int_{-\infty}^{+\infty}dt'f(t')W(t,t',\Omega,\sigma), \tag{12}$$

where t,Ω, and σ denote the time and harmonic frequency at which the window function is centered, and its temporal width, respectively. We consider a Gabor transform, for which the window function is given by

$$W(t,t',\Omega,\sigma)=\exp[-(t-t')^2/\sigma^2]\exp[i\Omega t']. \tag{13}$$

The usual Fourier transform $\mathcal{F}(\Omega)$, which yields no temporal information, is recovered for $\sigma\to\infty$. The temporal width σ corresponds to a frequency bandwidth $\sigma_\Omega=2/\sigma$. For a temporal width smaller than the period $T=2\pi/\omega$ of the driving field, the peaks in the time-resolved spectra $|\mathcal{F}(t,\Omega,\sigma)|^2$ yield the recombination times t_1. This method has been extensively used in the literature, in the three-step model framework [3].

III. GENERAL PICTURE

We shall now investigate the connection between HHG and the periodic level crossings in detail and draw a general physical picture of the mechanisms involved. The simplest physical situation for which one can do this is a monochromatic field

$$E(t)=E_0\sin(\omega t), \tag{14}$$

where E_0 and ω denote the field strength and frequency, respectively. In this case, the time t_c is given by the condition

$$\omega t_c=\frac{\omega_{10}}{2x_{10}E_0}. \tag{15}$$

If the field amplitude E_0 is large enough, then $\omega t_c\ll 1$, and the avoided crossings of the adiabatic states are well-separated. Thus the crossing times t_0 are well-defined and there is efficient population transfer at t_0. Hence one expects the corresponding spectrum to exhibit a wide plateau and a sharp cutoff.

The avoided crossings occur at the times $t_0=n\pi/\omega$ for which the field is vanishing. Thus one expects the population

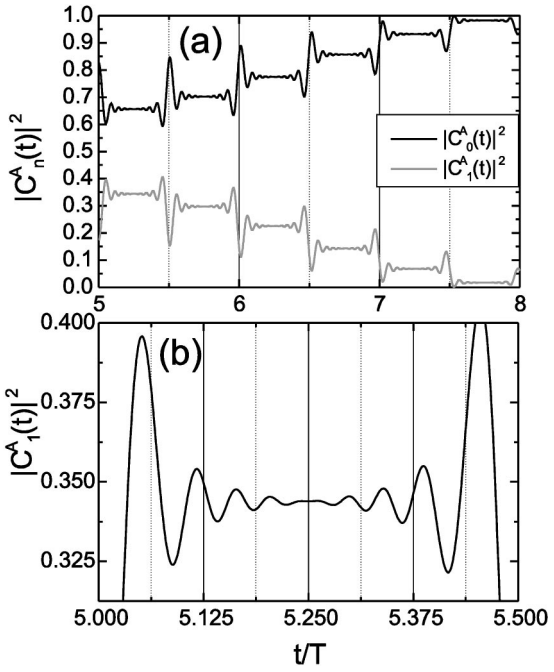

FIG. 1. Populations $|C_n^A(t)|^2$ of the adiabatic states as functions of time, for transition frequency $\omega_{10}=0.409$ a.u., external field parameters $\omega=0.05$ a.u., $E_0=0.6$ a.u., and dipole-matrix element $x_{10}=1.066$ a.u. Part (a) shows this feature for several cycles of the driving field, whereas part (b) depicts the population of the excited adiabatic state only within half a cycle. The times are given in units of the field cycle $T=2\pi/\omega$. The driving field is turned on linearly within two periods.

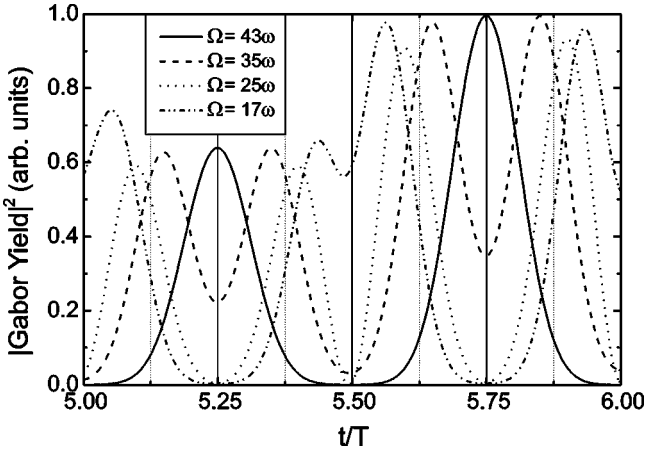

FIG. 2. Gabor spectra of the dipole acceleration [Eq. (11)] as functions of time, for field strength $E_0=1$ a.u., field frequency $\omega=0.05$ a.u., transition frequency $\omega_{10}=0.409$ a.u., and dipole matrix element $x_{10}=1.066$ a.u. The cutoff harmonic lies at $\Omega_M=43\omega$. The time width of the window function was chosen $\sigma=0.1T$. Its center was chosen at the cutoff harmonics, as well as at harmonic energies which roughly correspond to $\Omega=0.8\Omega_M$, $\Omega=0.6\Omega_M$, and $\Omega=0.4\Omega_M$. All time-resolved spectra have been normalized. The times are given in units of the field cycle $T=2\pi/\omega$. The driving field is turned on linearly within two periods.

transfers between the states $|\phi_n^A(t)\rangle$ to occur at these times. This is partially confirmed by Fig. 1, where the populations of the adiabatic states are plotted as functions of time. In fact, the pronounced peaks at the times t_0 clearly show that most population transfer takes place at these times. There are, however, several smaller peaks, which are symmetric with respect to the times $t_{1M}=(2n+1)\pi/2\omega$ for which the field is maximal. These peaks show that population transfer also occurs at other times, and can be seen in detail in Fig. 1(b).

The role of these population transfers in HHG can be understood using the Gabor transform of the dipole acceleration. The peaks in the Gabor spectra give the main contributions for high-order harmonic generation within a field cycle. For the cutoff harmonic, there is a single peak at t_{1M} which splits into two for the plateau harmonics. This peak gets further apart as the harmonic frequency decreases, varying from t_{1M} to the times at the immediate vicinity of the avoided crossings. These results are displayed in Fig. 2.

The physical interpretation of these features is rather simple. At the times the level crossings occur, i.e., at $t_0=nT/2$, there is a population transfer from the adiabatic state $|\phi_0^A(t)\rangle$ to $|\phi_1^A(t)\rangle$. The system remains in $|\phi_1^A(t)\rangle$ until a further time t_1, decaying back to $|\phi_0^A(t)\rangle$ and emitting a harmonic of frequency $\Omega=N\omega=\varepsilon_+^A-\varepsilon_-^A$. The explicit expression relating the time t_1 to the harmonic frequency would then be

$$\omega t_1=\arcsin[\pm\sqrt{(N\gamma_1)^2-(\gamma_2)^2}], \tag{16}$$

with $\gamma_1=\omega/(2x_{10}E_0)$ and $\gamma_2=\omega_{10}/(2x_{10}E_0)$. The physical significance of γ_1 and γ_2 will be discussed later in this paper (Sec. V). In order to obtain a harmonic at the maximum possible frequency Ω_M (i.e., the cutoff harmonic), the population transfer between the time-dependent states must occur at the times for which the energy difference $\varepsilon_+^A-\varepsilon_-^A$ is maximal, i.e., at $t_{1M}=(2n+1)\pi/2\omega$. As the harmonic energy decreases, there are two possible times for this population transfer to occur, a shorter and a longer one. The interference between these two possible quantum paths originates the well-structured two-level atom plateau, with sharp harmonic peaks. This process repeats itself every half cycle of the driving field. This picture is supported by the fact that all peaks in the time-resolved spectra satisfy Eq. (16) and thus can be traced back to population transfers between the adiabatic states. The times given by Eq. (16) for the parameters of Fig. 2, together with the corresponding harmonic energies, are written in Table I.

An analogous picture is observed within the three-step model framework. The cutoff harmonic can only be generated by an electron which returns to its parent ion with maximal kinetic energy. This maximal energy corresponds to a particular return time, which appears as a single peak in the Gabor yield. Within the plateau, there are two possible sets of electron trajectories corresponding to the same harmonic energy, such that this single peak splits into two [3]. In our case, the ''first step'' would be the population transfer from $|\phi_0^A(t)\rangle$ to $|\phi_1^A(t)\rangle$ at t_0, the ''second step'' would be the system following $|\phi_1^A(t)\rangle$ adiabatically in a time interval $\tau=t_1-t_0$, and the ''third step'' would be the population trans-

TABLE I. Level-crossing times t_0, population transfer times t_1, and the corresponding harmonic energy Ω for the parameters of Fig. 2. The times are given in units of the period $T=2\pi/\omega$. The harmonic orders, together with the approximate harmonic energies in units of the cutoff frequency Ω_M, are given in the remaining two columns. This pattern repeats itself every half-cycle of the driving field.

t_0/T	t_1/T	Harmonic order	Ω/Ω_M
0.5	0.25	43	1
0.5	0.14 0.36	35	0.8
0.5	0.09 0.41	25	0.6
0.5	0.05 0.45	17	0.4

fer from $|\phi_1^A(t)\rangle$ to $|\phi_0^A(t)\rangle$ at t_1, with subsequent harmonic generation. The corresponding physical picture is illustrated in Fig. 3.

Another interesting feature is that the population transfers between the adiabatic states are not strictly periodic within π/ω. Indeed, superposed to them, there are oscillations which occur within much larger time scales, their periods comprising several cycles of the driving field [29]. These oscillations are also present in the dipole length and acceleration as a global enveloping function, whose amplitude, form, and periodicity depend on the field strength E_0, the field frequency ω, and on the dipole matrix element x_{10} in a nontrivial way. These structures seem not to influence the harmonics globally, but mainly the substructure of the spectra and the hyper-Raman lines [30].

In Fig. 4, we show these enveloping functions for the populations of the adiabatic states [Fig. 4(a)], the dipole acceleration [Fig. 4(b)], and the Gabor spectra of the plateau and cutoff harmonics [Fig. 4(c)]. One should note that this enveloping function is the same for the Gabor transforms of all groups of harmonics displayed. Furthermore, it does not affect the splitting of the peaks, such that the population transfer times are always given by Eq. (16).

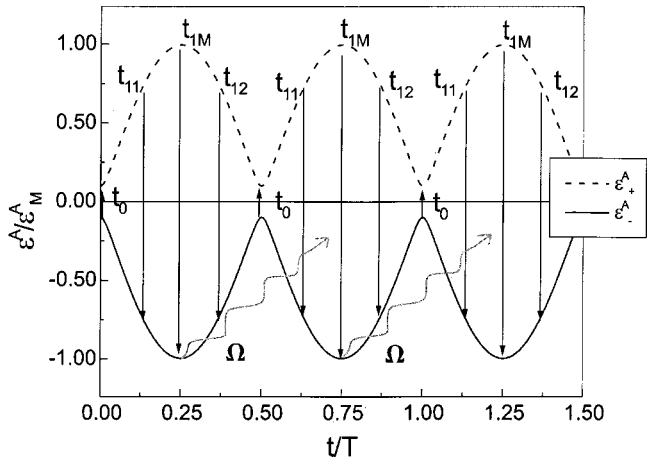

FIG. 3. Schematic representation of high-order harmonic generation in a two-level atom. The population transfers at the level crossings occur at the times t_0 and the main contributions to HHG occur at the times t_1. The times t_{1M}, t_{11}, and t_{12} correspond to the generation of the cutoff and plateau harmonics, respectively. The main physical processes are indicated by arrows in the figure, and the corresponding energies can be read in the vertical axis. The adiabatic energies are given in units of the maximal energy ε_M^A and the time in units of the field cycle. The field parameters are chosen in such a way that the ratio between the cutoff energy $\Omega_M=2\varepsilon_M^A$ and the transition frequency is $\Omega_M/\omega_{10}=10$.

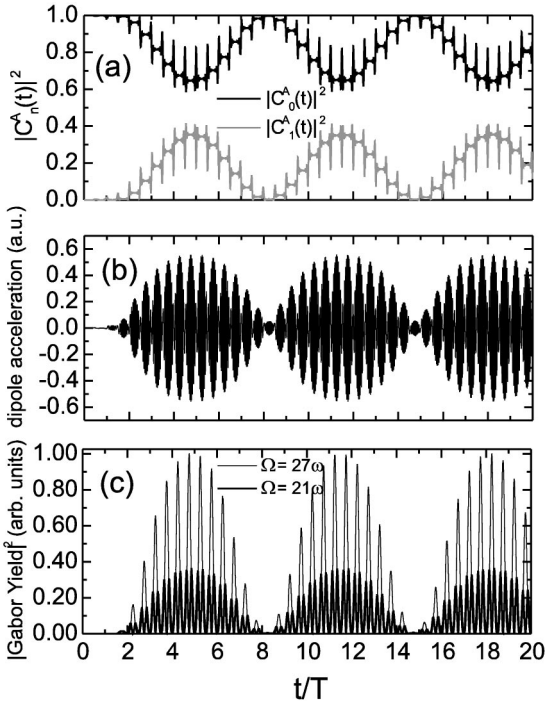

FIG. 4. Global structures as functions of time, for (a) the populations $|C_n^A(t)|^2$ of the adiabatic states, (b) the dipole acceleration $\ddot{x}(t)$, and (c) the Gabor spectra of the cutoff and plateau harmonics. The time width of the window function is $\sigma=0.1T$. The field strength, the field frequency, the transition frequency, and the dipole matrix element were chosen as $E_0=0.6$ a.u., $\omega=0.05$ a.u., $\omega_{10}=0.409$ a.u., and $x_{10}=1.066$ a.u., respectively. These parameters give $\gamma_1=0.0391$, $\gamma_2=0.3197$, and a cutoff frequency at $\Omega_{\max}=27\omega$. All Gabor spectra have been normalized to the maximum value obtained with the window function centered at the cutoff. The field is turned on linearly within two periods. The time is given in units of the field cycle.

IV. BICHROMATIC DRIVING FIELDS

In this section we consider a bichromatic driving field

$$E(t)=E_{01}\sin(\omega t)+E_{02}\sin(n\omega t+\theta), \tag{17}$$

with two main purposes. First, we wish to confirm the physical picture in which the main contributions to a particular set of harmonics, within a field cycle, occur at the times t_1 such that the corresponding harmonic frequency is the difference $\varepsilon_+^A-\varepsilon_-^A$ between the energies of the adiabatic states. Second, we are interested in understanding how an additional field can be used to distort the avoided crossings between the adiabatic states in such a way that the harmonic emission can be controlled. In the bichromatic case, depending on the field

parameters, the spectra may have several cutoffs, which are given by the maxima of $\varepsilon_+^A - \varepsilon_-^A$. Consequently, the main contributions to the generation of the cutoff harmonics take place at the times t_{1M} for which these maxima occur.

In order to obtain the level-crossing times t_0, as well as the times t_{1M}, one needs the extrema $\pm\varepsilon_M^A$ of the field-dressed energies $\varepsilon_\pm^A$. For the bichromatic field (17) they are given by

$$\cos(\omega t) + n\zeta\cos(n\omega t + \theta) = 0 \tag{18}$$

and

$$\sin(\omega t) + \zeta\sin(n\omega t + \theta) = 0, \tag{19}$$

where $\zeta = E_{02}/E_{01}$ denotes the field-strength ratio. Equation (18) gives the extrema which coincide with those of the field, and therefore t_{1M}, whereas Eq. (19) gives those which correspond to the avoided crossings, and therefore t_0. Depending on the frequency ratio n, the field-strength ratio ζ, and the relative phase θ, these times, as well as the corresponding extrema, can be very different. In this paper we will provide concrete examples for a $\omega - 2\omega$ field, i.e., with $n = 2$, relative phases $\theta_1 = 0$ and $\theta_2 = \pi/2$, and arbitrary ζ. For these specific parameters, Eqs. (18) and (19) have a simple form, with analytical solutions.

A. Relative phase $\theta = 0$

In this case, Eq. (18) reduces to

$$\cos^2(\omega t) + \frac{1}{4\zeta}\cos(\omega t) - \frac{1}{2} = 0, \tag{20}$$

which yields two sets of times, namely

$$t_{1M} = \frac{1}{\omega}\arccos\left(-\frac{1}{8\zeta} \pm \frac{1}{2}\sqrt{\frac{1}{16\zeta^2} + 2} \right). \tag{21}$$

The solutions corresponding to the positive root exist for all field-strength ratios, whereas the remaining solutions are only present for $\zeta > 0.5$. Further in this section, it will be shown that the first set gives the absolute maxima of $\varepsilon_\pm^A$, which correspond to the cutoff in the harmonic spectra, whereas the second set yields local maxima at much lower energies.

The expression giving the avoided crossings, on its turn, can be written as

$$\sin(\omega t)[1 + 2\zeta\cos(\omega t)] = 0. \tag{22}$$

This equation yields the crossing times $t_0 = n\pi/\omega$, and $t_0' = (1/\omega)\arccos[-1/(2\zeta)]$. The crossing times t_0 do not depend on the field-strength ratio and are the same as in the monochromatic case, whereas the crossing times t_0' clearly do. Furthermore, these latter times are only present for $\zeta > 0.5$.

Figure 5 gives concrete examples of how the adiabatic energies $\varepsilon_\pm^A$ depend on time, for different field-strength ratios. In contrast to the monochromatic case, $\varepsilon_\pm^A$ is not periodic within half a cycle of the driving field. This is not surprising, since the periodicity of the field-dressed energies is effectively determined by $E^2(t)$ [cf. Eq. (7)]. For a monochromatic field, $E^2(t) = E^2(t + \pi/\omega)$ always holds, whereas in the bichromatic case this is only true for odd frequency ratios n. This is clearly *not* the case addressed in this paper. For the phase $\phi = 0$, one observes that $\varepsilon_\pm^A(t) = \varepsilon_\pm^A(2\pi/\omega - t)$, if both times are taken symmetrically with respect to $t_0 = n\pi/\omega$. This property already reflects itself in the expressions for t_0, t_{1M}, and t_0' derived in this section.

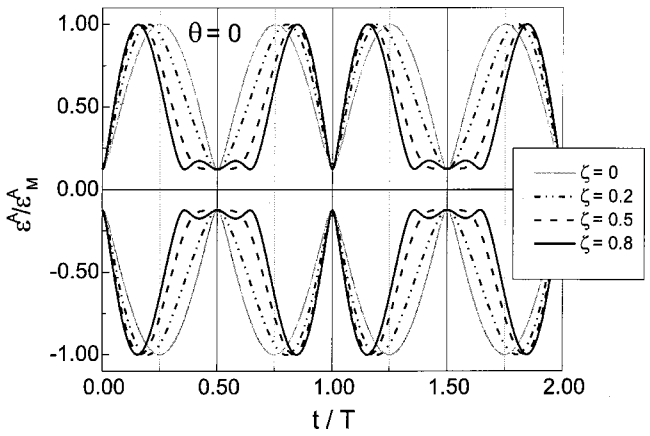

FIG. 5. Energies of the adiabatic states for a bichromatic field $E(t) = E_{01}\sin(\omega t) + E_{02}\sin(2\omega t + \theta)$, for $\theta = 0$ and several field-strength ratios $\zeta = E_{02}/E_{01}$. The time t is given in units of the field cycle $T = 2\pi/\omega$ and the field-dressed energies in units of the maximal energy ε_M^A. The field parameters were chosen such that $\Omega_M/\omega_{10} = 8$.

Furthermore, one clearly sees that, as predicted in Eq. (22), for $\zeta < 0.5$, the second driving wave only distorts the avoided crossings, making them broader at $t_0 = (2n + 1)\pi/\omega$ and sharper at $t_0 = 2n\pi/\omega$. For $\zeta = 0.5$, the broad crossing starts to split, originating the crossings given at the times t_0'. This splitting also leads to the second set of maxima predicted by Eq. (21), which corresponds to a set of harmonics of relatively low frequencies.

One must now understand which consequences this effect has on the physical quantities involved. With that purpose, we choose the strengths of both driving waves such that ε_M^A, and therefore the cutoff energy, remains unchanged and is equal to the monochromatic cutoff energy, for variable field-strength ratio ζ. This gives

$$E_{01} = \frac{E_0}{\sqrt{1 - \beta^2}(1 + 2\beta\zeta)}, \tag{23}$$

with $\beta = \cos(t_{1M})$.

The population transfers between the adiabatic states, as functions of time, also exhibit very similar asymmetries to the ones observed in the field-dressed energies. The population transfers at the broad crossings, for instance, take place at longer time intervals than those at the sharp crossings, making the oscillations in $|C_n^A(t)|^2$ asymmetric with respect to the times t_{1M}. This asymmetry increases with increasing ζ. An example is provided in Fig. 6(a). A similar feature

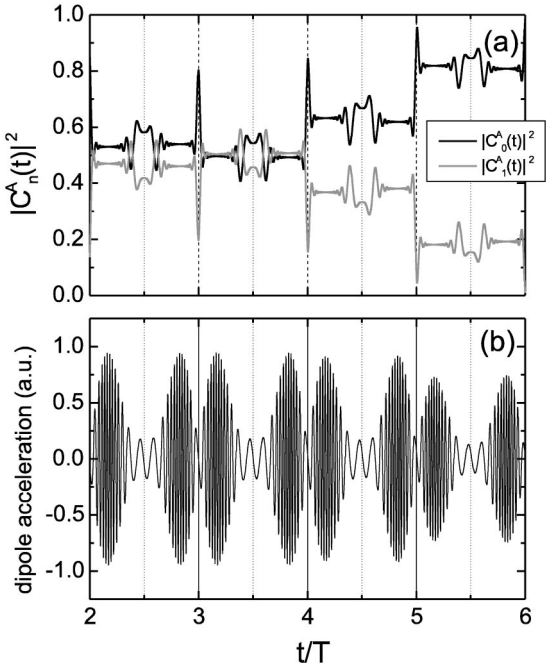

FIG. 6. Populations $|C_n^A(t)|^2$ of the adiabatic states [part (a)] and dipole acceleration [part (b)] as functions of time, for a bichromatic field $E(t)=E_{01}\sin(\omega t)+E_{02}\sin(2\omega t+\theta)$, with $\theta=0$, $\omega=0.05$ a.u., $\omega_{10}=0.409$ a.u., $x_{10}=1.066$ a.u., and field-strength ratio $\zeta=E_{02}/E_{01}=0.5$. The field amplitudes were chosen according to Eq. (23), with $E_0=1$ a.u. The time t is given in units of the field cycle.

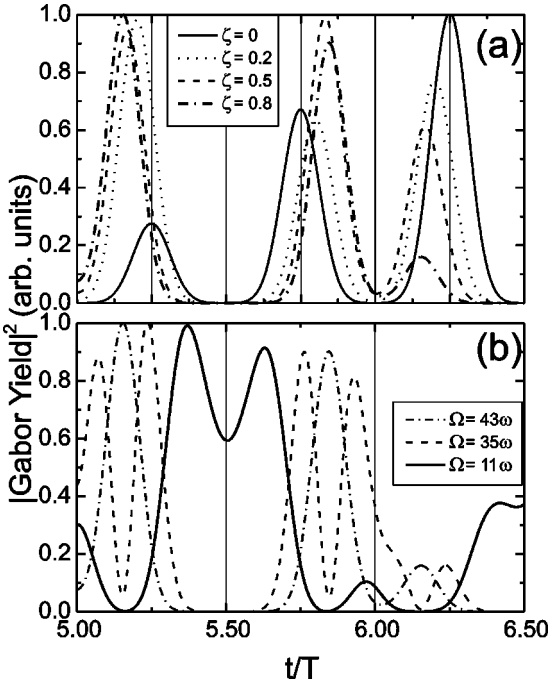

FIG. 7. Gabor spectra of the dipole acceleration as functions of time, for a bichromatic field $E(t)=E_{01}\sin(\omega t)+E_{02}\sin(2\omega t+\theta)$, with $\theta=0$, $\omega=0.05$ a.u., $\omega_{10}=0.409$ a.u., $x_{10}=1.066$ a.u., and several field-strength ratios $\zeta=E_{02}/E_{01}$. The maximal field strength is kept fixed according to Eq. (23), with $E_0=1$ a.u. The cutoff energy lies at $\Omega_M=2\varepsilon_M^A=43\omega$. The temporal width of the window function is $\sigma=0.1T$. In part (a), the window function is centered at the cutoff harmonics, and the field-strength ratio is $0\leqslant\zeta\leqslant 0.8$. In part (b), the center of the window function is taken for different frequencies, and $\zeta=0.8$. All curves in the figure have been normalized to their maximum values.

occurs for the dipole acceleration. This highly oscillating function exhibits nodes at the level-crossing times. In the monochromatic case, these nodes extend over identical temporal regions every half-cycle of the driving field. For bichromatic fields, however, with the distortion of the crossings by the second driving wave, this picture changes. There exist narrower and broader nodal regions, corresponding to the narrower and broader crossings, respectively. Thus the oscillations of the dipole acceleration get ''squeezed'' between the broader nodes. This feature can be seen in Fig. 6(b).

The Gabor transform of the dipole acceleration, taken at the cutoff and in the plateau, confirms this picture. In Fig. 7(a) there is a clear displacement of the peaks in the time-resolved spectra for the cutoff harmonics, with respect to the monochromatic case, and these peaks occur at the times predicted by Eq. (21). Similarly to the monochromatic case, these peaks split into two in the plateau region, being, however, slightly asymmetric [Fig. 7(b)]. This asymmetry is related to the above-mentioned difference in the shapes of the crossings. Furthermore, for a larger field-strength ratio, the additional times can also be seen for a group of harmonics at the low-energy end of the plateau. The times t_0 and t_{1M}, together with the respective cutoff energies, are given in Table II for the specific parameters considered in this figure.

B. Relative phase $\theta=\pi/2$

For this relative phase, Eq. (18) has the form

$$\cos(\omega t)[1-2\zeta\sin(\omega t)]=0. \tag{24}$$

This equation has two types of solutions: $t_{1M}=(n+1/2)\pi/\omega$, which do not depend on the field-strength ratio and yield the same maxima as in the monochromatic case, and $t'_{1M}=1/\omega\arcsin[1/(4\zeta)]$, which clearly depend on ζ and exist only for $\zeta\geqslant 0.25$. This already hints at a completely different situation as in the previous section, which will now

TABLE II. Times for the population transfers between the extrema of the adiabatic states, with the approximate order of the corresponding cutoff harmonic, for a bichromatic field given by Eq. (17), with relative phase $\theta=0$ and several field-strength ratios $\zeta=E_{02}/E_{01}$. The field and two-level atom parameters are the same as those used in Fig. 7. No entry means that the corresponding maxima do not exist. This pattern repeats itself every cycle $T=2\pi/\omega$ of the driving field.

$\zeta=0.2$			$\zeta=0.5$			$\zeta=0.8$		
t_0/T	t_{1M}/T	Ω_M/ω	t_0/T	t_{1M}/T	Ω_M/ω	t_0/T	t_{1M}/T	Ω_M/ω
0	0.20	43	0	0.17	43	0	0.15	43
0.5	0.80	43	0.5	0.83	43	0.36	0.42	9
						0.5	0.85	43
						0.64	0.58	9

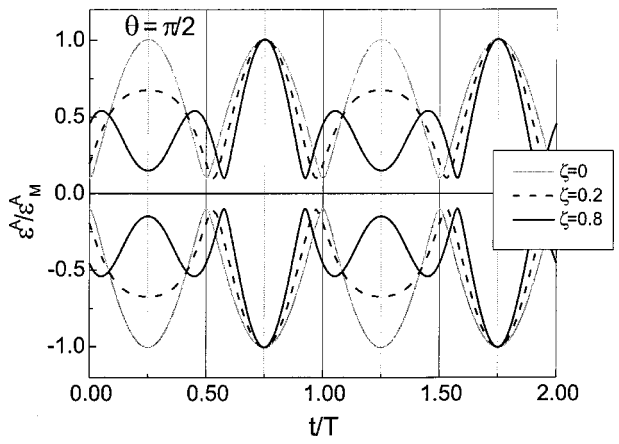

FIG. 8. Energies of the adiabatic states for a bichromatic field $E(t)=E_{01}\sin(\omega t)+E_{02}\sin(2\omega t+\theta)$, for $\theta=\pi/2$ and several field-strength ratios $\zeta=E_{02}/E_{01}$. The time t is given in units of the field cycle and the field-dressed energies in units of the maximal energy $\varepsilon^A_{M_2}$. The field parameters were chosen such that $\Omega_{M_2}/\omega_{10}=8$. The times t_{1M_i} are indicated in the figure by the dotted and solid grid lines, respectively.

be discussed in detail. This also holds for the times at which the avoided crossings occur. They must now satisfy

$$\sin^2(\omega t)-\frac{1}{2\zeta}\sin(\omega t)-\frac{1}{2}=0, \tag{25}$$

such that

$$t_0=\frac{1}{\omega}\arcsin\left(\frac{1}{4\zeta}\pm\frac{1}{2}\sqrt{\frac{1}{4\zeta^2}+2}\right), \tag{26}$$

all of them depending on ζ. This means that, in contrast to the case $\theta=0$, one may shift all level-crossing times by changing the relative intensities of the driving waves. The set of crossings given by the positive root in Eq. (26) exists only for $\zeta\geqslant 1$, whereas the remaining crossings occur for all ζ.

In Fig. 8 we depict the adiabatic states as functions of time, for several values of ζ, similarly to what was done for $\theta=0$. This figure illustrates how the relative phase can radically alter the whole physical picture. For $\theta=\pi/2$, already a relatively weak high-frequency wave considerably distorts the avoided level crossings, as well as the maxima of the field-dressed energies. An interesting feature is that the avoided crossings now move with the field-strength ratio. Furthermore, the maximal energies are no longer equal, but, within a field cycle, there are two comparable and different cutoff energies. This can be directly seen by computing the extrema of the energies $\varepsilon^A_{\pm}$, which occur for t_{1M}.

For field-strength ratio $\zeta<0.25$, they give the energies

$$\varepsilon^A_{M_1}=\frac{1}{2}\sqrt{\omega_{10}^2+4x_{10}^2(E_{01}-E_{02})^2} \tag{27}$$

and

$$\varepsilon^A_{M_2}=\frac{1}{2}\sqrt{\omega_{10}^2+4x_{10}^2(E_{01}+E_{02})^2}, \tag{28}$$

which correspond to the times $t_{1M_1}=0.25T \bmod \mathrm{T}$, and to $t_{1M_2}=0.75T \bmod \mathrm{T}$, respectively. These times define symmetry axes for the time-dependence of the adiabatic energies.

For $\zeta\geqslant 0.25$, a further splitting of the set of maxima at t_{1M_1} occurs, as predicted in Eq. (24). There exist now two sets of maxima, at the times t'_{1M}, whose energies are equal and given by

$$\varepsilon^A_{M_1}=\frac{1}{2}\sqrt{\omega_{10}^2+4x_{10}^2E_{01}^2\frac{(1+8\,\zeta^2)^2}{64\,\zeta^2}}. \tag{29}$$

These maxima are symmetric with respect to t_{1M_1}. For these times, the adiabatic energies now exhibit a minimum. This causes, for large ζ, additional avoided crossings (cf. Fig. 8 for $\zeta=0.8$). The population transfers at these times are, however, small, and play only a secondary role in the problem addressed in this paper. For the sake of simplicity, even after the second splitting, we shall refer to the lower-energy set of maxima as $\varepsilon^A_{M_1}$. The other set of maxima does not split, and the corresponding times t_{1M_2} remain constant for all ζ. One should note that the adiabatic energies, in the $\theta=\pi/2$ case, satisfy $\varepsilon^A_{\pm}(t)=\varepsilon^A_{\pm}(T/2-t)$, if both times are chosen symmetrically with respect to t_{1M_1} or t_{1M_2}. This also holds for the population-transfer times derived in this section.

In order to investigate how the distortions in the adiabatic-state energies influence the physical quantities of interest, we shall keep the cutoff energy $\Omega_{M_2}=2\varepsilon^A_{M_2}$ fixed, and equal to the cutoff energy of the monochromatic case. Thus the field strengths E_{01} and E_0 are related by

$$E_{01}=\frac{E_0}{1+\zeta}. \tag{30}$$

As in the previous section, we can trace all distortions observed in these physical quantities back to those observed in time dependence of $\varepsilon^A_{\pm}$. For instance, the shifts in the level-crossing times t_0 predicted by Eq. (26) are also present in the main population-transfer times for the adiabatic states [Fig. 9(a)] and in the nodes of the dipole acceleration [Fig. 9(b)]. Another effect which is clearly seen in both quantities is the splitting of the maxima near $t_{1M_1}=0.25T \bmod \mathrm{T}$. Indeed, there exist now two sets of maxima which are symmetric with respect to these times, for $\zeta\geqslant 0.25$.

We now investigate the Gabor transform of the cutoff and plateau harmonics. In Fig. 10(a) we display the time-resolved spectra, centered at the harmonic frequencies $\Omega_{M_2}=2\varepsilon^A_{M_2}$, for different field-strength ratios ζ. The monochromatic case is also displayed for comparison. As a general feature, for $\zeta\neq 0$, the peaks of the Gabor spectra at $t_{1M_1}=0.25T \bmod \mathrm{T}$ vanish. This is a direct consequence of the splitting of the extrema of the adiabatic energies caused by the high-frequency wave. Due to this splitting, the energy

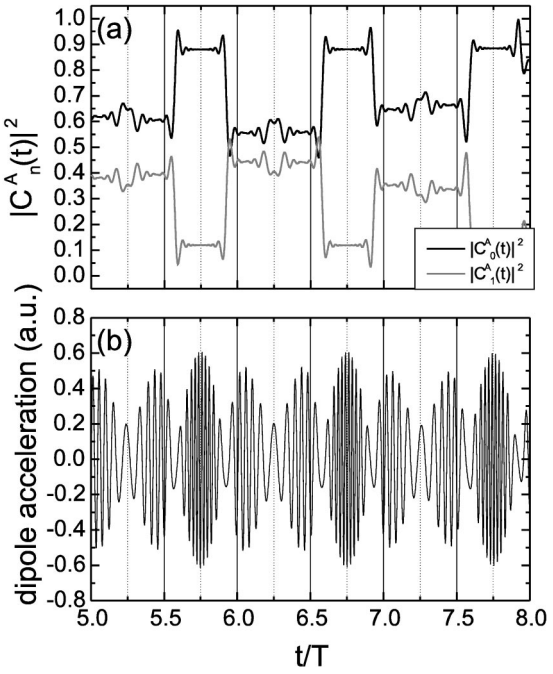

FIG. 9. Populations $|C_n^A(t)|^2$ of the adiabatic states [part (a)] and dipole acceleration [part (b)] as functions of time, for a bichromatic field $E(t)=E_{01}\sin(\omega t)+E_{02}\sin(2\omega t+\theta)$, with $\theta=\pi/2$, $\omega=0.05$ a.u., $\omega_{10}=0.409$ a.u., $x_{10}=1.066$ a.u., and field-strength ratio $\zeta=E_{02}/E_{01}=0.8$. The time t is given in units of the field cycle.

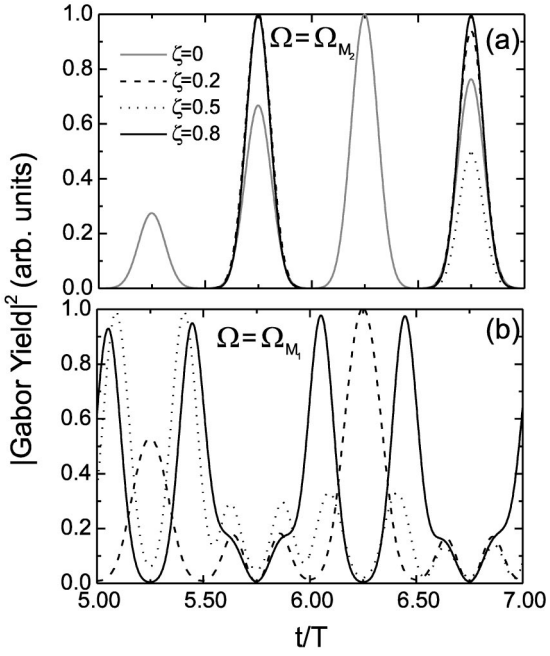

FIG. 10. Gabor spectra of the dipole acceleration as a function of time, for a bichromatic field $E(t)=E_{01}\sin(\omega t)+E_{02}\sin(2\omega t+\theta)$, with $\theta=\pi/2$, $\omega=0.05$ a.u., $\omega_{10}=0.409$ a.u., $x_{10}=1.066$ a.u., and several field-strength ratios $\zeta=E_{02}/E_{01}$. The maximal field strength is kept fixed according to Eq. (30) and equal to $E_0=1$ a.u. The upper-cutoff energy lies at $\Omega_{M_2}=43\omega$. The lower-cutoff energy varies with ζ. All cutoff energies are given in Table III, together with the population transfer times t_0 and t_{1M_2}. In part (a), the window function is centered at the upper-cutoff harmonics ($\Omega_{M_2}=2\varepsilon^A_{M_2}$), and the field-strength ratio is $0\leqslant\zeta\leqslant0.8$. In part (b), the center of the window function is taken at $\Omega_{M_1}=2\varepsilon^A_{M_1}$. All curves have been normalized to their maximum values. In part (a), the monochromatic case is also displayed for comparison.

maxima near t_{1M_1} lie outside the range of the window function and do not contribute to the time-resolved spectra. Furthermore, as predicted in Eq. (25), the peaks at the maxima $t_{1M_2}=0.75T$ mod T do not move in time as ζ is varied.

Taking now the window function (13) centered at $\Omega_{M_1}=2\varepsilon^A_{M_1}$ [Fig. 10(b)], one observes, as expected, a completely different behavior for the peaks near $t_{1M_1}=0.25T$ mod T. For $\zeta<0.25$, these peaks are exactly at these times. For $\zeta\geqslant0.25$, as expected, they now occur at $t'_{1M}=1/\omega\arcsin[1/(4\zeta)]$, which vary with the field-strength ratio ζ. Furthermore, this second set of peaks splits for these larger field-strength ratios, such that two sets of peaks which are symmetric with respect to t_{1M_1} are now present. Other sets of peaks which can be seen in the picture correspond to the upper-plateau return times, which occur for $\Omega<\Omega_{M_2}$ and are symmetric with respect to $t_{1M_2}=0.75T$ mod T. These peaks come from the splitting of t_{1M_2}, which occurs in this energy range (cf. Fig. 8). The population-transfer times for the specific parameters of this figure, together with the corresponding harmonic frequencies, are given in Table III.

C. Fourier spectra for the two phases

In the investigations performed so far, our main objective was to understand how an additional driving wave may distort the time dependence of the adiabatic energies and the time profile of harmonic generation. In this section, we address the question of how these distortions influence the harmonic spectra. Furthermore, we are interested in extending the cutoff, and, by doing so, guaranteeing that the harmonics in this energy region are strong enough for applicational purposes. Clearly, the ideal scenario is to extend the cutoff en-

TABLE III. Times for the population transfers between the extrema of the adiabatic states, with the approximate order of the corresponding cutoff harmonic, for a bichromatic field given by Eq. (17), with relative phase $\theta=\pi/2$ and several field-strength ratios $\zeta=E_{02}/E_{01}$. The field and two-level atom parameters are the same as those used in Fig. 10. No entry means that the corresponding maxima do not exist. This pattern repeats itself every cycle $T=2\pi/\omega$ of the driving field. For $\zeta=0.8$, there are additional avoided crossings at $0.25T$ mod T.

$\zeta=0.2$			$\zeta=0.5$			$\zeta=0.8$		
t_0/T	t_{1M}/T	Ω_M/ω	t_0/T	t_{1M}/T	Ω_M/ω	t_0/T	t_{1M}/T	Ω_M/ω
0.53	0.75	43	0.56	0.75	43	0.58	0.75	43
0.97	1.25	30	0.94	1.08	23	0.92	1.05	24
			0.94	1.42	23	0.92	1.45	24
						1.25	1.45	24

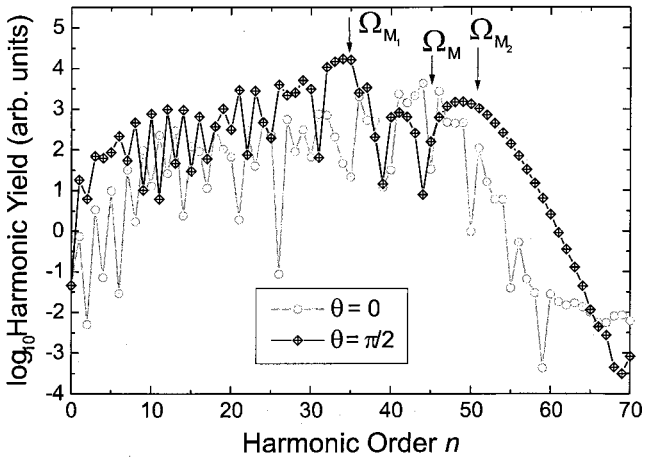

FIG. 11. Spectra computed from the dipole acceleration, for the bichromatic field $E(t)=E_{01}\sin(\omega t)+E_{02}\sin(2\omega t+\theta)$, for $\theta=0$, $\theta=\pi/2$, and field strengths $E_{01}=1.0$ a.u. and $E_{02}=0.2$ a.u. The field is switched on linearly within two cycles. The remaining parameters are $\omega=0.05$ a.u., $\omega_{10}=0.409$ a.u., $x_{10}=1.066$. The cutoff frequency for $\theta=0$ is roughly at $\Omega_M=46\omega$, whereas for $\theta=\pi/2$ the cutoff frequencies are approximately at $\Omega_{M_1}=35\omega$ and $\Omega_{M_2}=52\omega$. All cutoff energies are indicated by arrows in the figure.

ergy without any intensity loss in the corresponding harmonic range.

With that purpose, we keep E_{01} and E_{02} fixed and compare spectra obtained for $\theta_1=0$ and $\theta_2=\pi/2$. These results are displayed in Fig. 11. As a global feature, one observes that, for $\theta=0$, all harmonics behave in a very similar way, with no distinct regions, as for instance a double plateau, in the spectra. This is related to the fact that no splitting of the cutoff energy occurs in this case. The two maxima in $\varepsilon_{\pm}^{A}$ have the same energy, even though the level-crossing pattern is no longer periodic in $T/2$. On the other hand, for $\theta=\pi/2$, there is a clear double-plateau structure. In fact, one can identify a completely different physical behavior for the harmonics in the frequency regions $\Omega<\Omega_{M_1}$ and $\Omega_{M_1}<\Omega<\Omega_{M_2}$. The double-plateau structure is due to the different cutoff energies which exist in the $\theta=\pi/2$ case.

Another generic feature is that the cutoff energy is extended for $\theta=\pi/2$. This is expected, since this quantity is given by the maximum energy difference between the adiabatic states. For a field given by Eq. (17), the maximal possible energy is obtained for $E(t_{1M_2})=E_{01}+E_{02}$. This yields the harmonic frequency Ω_{M_2}, discussed in the previous section.

There exist, however, nongeneric features, which depend on the absolute field parameters, as, for instance, its strength. Examples of such features are the intensity ratio between the upper and lower parts of the plateau for $\theta=\pi/2$, and the intensities of the harmonics obtained for $\theta=\pi/2$, compared to those obtained for $\theta=0$. Thus, depending on the absolute parameters used, it is not always possible to extend the cutoff energy without loss of intensity. In order to control HHG in a two-level atom in a more reliable way, a more detailed study of these features for the particular system in question is necessary.

These nongeneric features are mainly due to the fact that the population transfer at the level crossings is, in general, given by more complicated expressions than in the monochromatic case. Indeed, these expressions depend on the shape and width of the crossing, and on the duration of the interaction. These shapes have been studied in [28,31]. Furthermore, the global structures of the adiabatic-state populations $|C_n^A(t)|^2$ have a stronger influence on the spectra in the bichromatic case than for monochromatic driving fields.

Thus the physical picture discussed in Sec. III holds in a more general framework, as, for instance, bichromatic driving fields. Nevertheless, the distortions in the level crossings caused by additional fields may have consequences in the quantities involved, including the spectra, which are difficult to predict. This does not mean that control cannot be performed at all, but, rather, that it can be done in a restricted context. In fact, one still has a very good predictive power over generic features, as, for instance, the double plateau or the cutoff energies indicated in Fig. 11.

V. SCALING BEHAVIOR

In the results discussed in the previous sections, we have used rather unrealistic frequencies and intensities for the driving fields, for which most physical systems would ionize immediately. This choice of parameters allows us to obtain results with very little numerical effort. In order to extend our computations to more realistic cases, as, for instance, solids, there are two possibilities. Either one slightly increases the effort to obtain the necessary precision, or one must find specific combinations of parameters for which the physical quantities involved remain invariant. This second approach has the advantage of providing additional insight into the physics of the problem.

With that purpose, we analyze the scaling behavior of these quantities. We use scaling laws which have been derived elsewhere [32], in the context of stabilization of atoms in strong laser fields. We concentrate on the question of whether driving fields of much lower frequencies and intensities could originate similar spectra, with, for instance, the same number of harmonics, or the same population-transfer times, in units of the field cycle. Therefore our starting point will be the expression

$$\sin(\omega t_1)+\zeta\sin(n\omega t_1+\theta)=\pm\sqrt{(N\gamma_1)^2-(\gamma_2)^2}, \quad (31)$$

which relates the harmonic energy to the energy difference of the adiabatic states. This equation gives the population-transfer times. For $\zeta=0$, one has the monochromatic-field case [Eq. (16)], and, for $\zeta\neq 0$ and $n=2$, the bichromatic situation discussed in the previous section. Note that the parameters E_0, ω, ω_{10}, and x_{10} appear combined, as $\gamma_1=\omega/(2x_{10}E_0)$, or $\gamma_2=\omega_{10}/(2x_{10}E_0)$. The denominators of these expressions give the Rabi frequencies $\Omega_R=2x_{10}E_0$, which scale like the energies [cf. Eqs. (3) and (6) for the two-level Hamiltonian]. This keeps the Schrödinger equation invariant under scale transformations.

We now consider the scale transformation

$$\omega \rightarrow \omega' = \lambda\omega; \quad \omega_{10} \rightarrow \omega'_{10} = \lambda\omega_{10}; \quad \Omega_R \rightarrow \Omega'_R = \lambda\Omega_R, \tag{32}$$

where λ denotes the dilatation factor. The invariance of the Schrödinger equation also requires that the time scales as $t \rightarrow t' = \lambda^{-1}t$, such that Eq. (31) will remain invariant.

This apparently trivial result has far-reaching consequences. In fact, it shows that, for *any* set E_0, ω, ω_{10}, and x_{10}, the number of harmonics N in the spectra and the corresponding population-transfer times $\tilde{t}_1 = \omega t_1/(2\pi)$, given in terms of field cycles, remain invariant, as long as γ_1 and γ_2 are kept constant.

Since the unitary transformation (5) which gives the adiabatic states also depends on E_0, ω, ω_{10}, and x_{10} through γ_1 and γ_2, it also remains invariant in this case. Thus this invariance must also hold for the populations of these states, i.e., $|C_n^A(t)|^2 = |C_n^A(t')|^2$.

Another quantity of interest is the dipole acceleration. A quick inspection of Eq. (11) shows that this quantity does not remain invariant under the above-stated transformations. In fact, it scales as x_{10} multiplied by the square of the energy. The dipole matrix element scales as $x_{10} \rightarrow x'_{10} = \lambda^{-1/2}x_{10}$. Thus $\ddot{x}(t) = \lambda^{3/2}\ddot{x}(t')$.

The above-stated conclusions are confirmed by Fig. 12. In this figure, we display the same physical quantities as in Fig. 4 for a completely different set of parameters which, however, yield the same γ_1 and γ_2. The populations $|C_n^A(t)|^2$, in this case [cf. Fig. 12(a)] are, as expected, identical to those depicted in Fig. 4. This is true not only for the oscillations which are periodic in $T/2$, but also for the global enveloping functions. The scaling with $\lambda^{3/2}$ is also observed for the dipole acceleration [Fig. 12(b)]. The parameters used in the figure are typical for quantum wells and solid-state systems [24].

Another interesting aspect concerns the resulting harmonic spectra. Even though, in absolute terms, these spectra have different cutoff frequencies and different global intensities, for equal γ_1 and γ_2 they have the same shape. Not only the number of harmonics is the same. In addition, all substructure in the spectra looks strikingly similar. These features can be easily understood: the global intensity decrease is related to the decrease in amplitude of the dipole acceleration and the identical shapes are a consequence of the fact that the populations of the adiabatic states, as well as all oscillations present in the dipole acceleration, remain invariant under the scale transformations discussed here. This is shown in Figs. 13(a) and 13(b) for several dilatation factors λ. The corresponding field and two-level atom parameters are given in Table IV.

On the other hand, the behavior of the system can already be altered by small variations in γ_1 and γ_2. For instance, in Fig. 14 we consider a slightly larger field amplitude than in Fig. 4, which gives different γ_1 and γ_2. In this case, one observes a radically different pattern for the populations $|C_n^A(t)|^2$ [Fig. 14(a)] and the dipole acceleration [Fig. 14(b)].

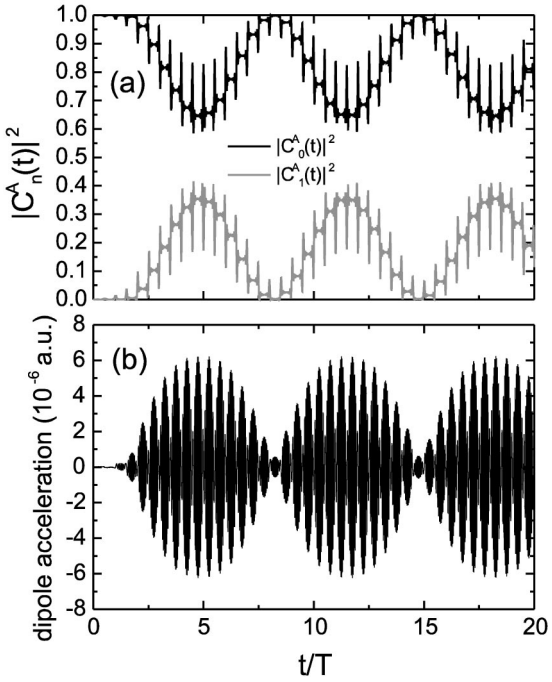

FIG. 12. Global structures as functions of time, for (a) the populations $|C_n^A(t)|^2$ of the adiabatic states and (b) the dipole acceleration $\ddot{x}(t)$. The field strength, the field frequency, the transition frequency, and the dipole matrix element were chosen as $E_0 = 6.71 \times 10^{-6}$ a.u., $\omega = 2.5 \times 10^{-5}$ a.u., $\omega_{10} = 2.045 \times 10^{-5}$ a.u., and $x_{10} = 47.673$ a.u., respectively. These parameters are typical for solid-state systems and give $\gamma_1 = 0.0391$, $\gamma_2 = 0.3197$, which are the same as in Fig. 4. They are obtained from those in Fig. 4 using a scaling transformation with $\lambda = 1/2000$. For this set of parameters, we have used a five times smaller time step than in the previous figures and double precision. The dipole acceleration is given in atomic units and the time is given in units of the field cycle. The field is switched on linearly within two cycles.

As a direct consequence, the spectra do not exhibit the same substructure [Figs. 15(a) and 15(b)].

VI. CONCLUSIONS

The results discussed in the previous sections lead to the main conclusion that the three-step model and the two-level atom are not completely different physical pictures for describing high-order harmonic generation, as commonly believed. Indeed, in both models, this phenomenon takes place as a result of a three-step process. Hints that a correspondence between both physical pictures might exist have been provided in the literature [14,20]. We go, however, beyond such studies, giving evidence that a three-step mechanism exists in the two-level atom case and analyzing its features in detail.

In the usual form of the three-step model, there is population transfer from the atomic ground state to a state in the continuum, i.e., tunneling or multiphoton ionization. The electron then propagates in the continuum within a time interval $\tau = t_1 - t_0$, gaining a certain amount of kinetic energy which is converted into harmonic radiation at a time t_1, when

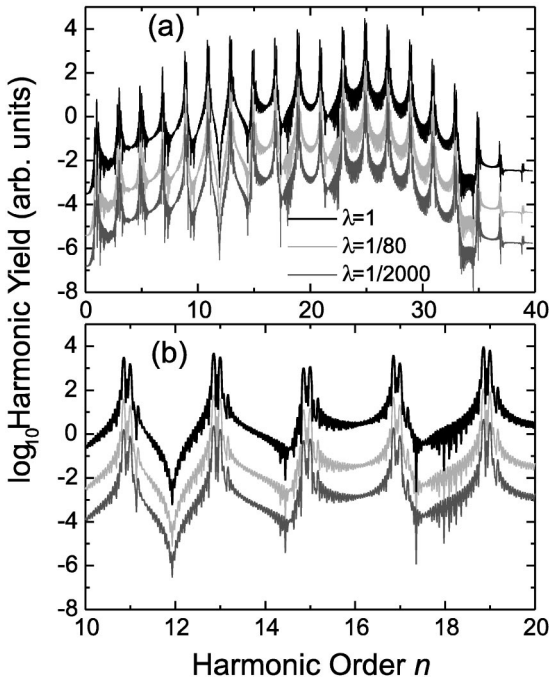

FIG. 13. Harmonic spectrum for the same parameters as in Fig. 4 ($\lambda=1$), compared to those obtained for several field strengths E_0, field frequencies ω, transition frequencies ω_{10}, and matrix dipole elements x_{10}, chosen such that $\gamma_1=0.0391$ and $\gamma_2=0.3197$, i.e., the same as in Fig. 4. These parameters are displayed in Table IV. Part (a) shows the whole spectra, whereas part (b) displays both spectra for harmonic order $10<N<20$, such that their substructure can be seen. The field is switched on linearly within two cycles.

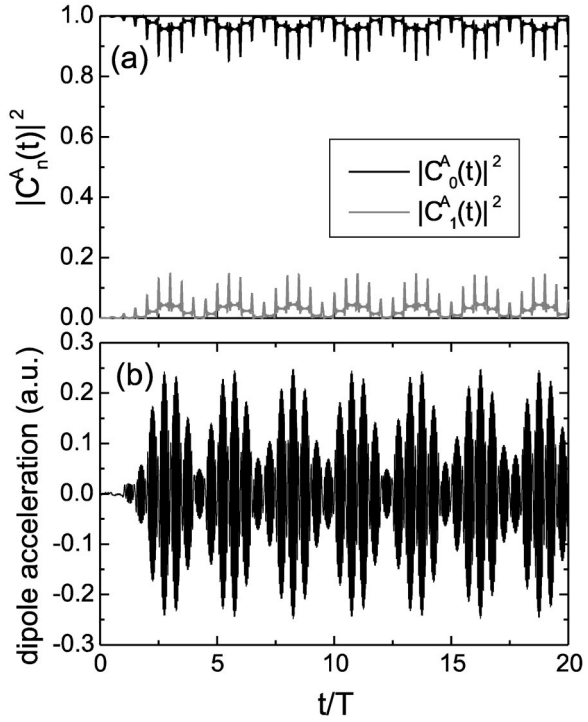

FIG. 14. Global structures as functions of time, for (a) the populations $|C_n^A(t)|^2$ of the adiabatic states and (b) the dipole acceleration $\ddot{x}(t)$. The field strength, the field frequency, the transition frequency, and the dipole matrix element were chosen as $E_0=0.62$ a.u., $\omega=0.05$ a.u., $\omega_{10}=0.409$ a.u., and $x_{10}=1.066$ a.u., respectively. These parameters are slightly different from the ones in Fig. 4, but give $\gamma_1=0.0378$, $\gamma_2=0.3094$. The field is switched on linearly within two cycles. The time is given in units of the field cycle.

there is population transfer from the continuum to the ground state, i.e., recombination. In the two-level atom framework, a very similar process takes place: there is population transfer from the field-dressed state $|\phi_0^A(t)\rangle$ to the state $|\phi_1^A(t)\rangle$ at a time t_0 for which an avoided crossing occurs. Subsequently, the system acquires energy from the field within the interval $\tau=t_1-t_0$, and, at a further time t_1, when population transfer from $|\phi_1^A(t)\rangle$ back to $|\phi_0^A(t)\rangle$ takes place, this energy is released in the form of harmonic radiation. Thus the main difference between the three-step model and the two-level atom physical pictures is that in the latter case, the three steps do not involve a continuum state, but a field-dressed bound state.

Further similarities are observed in the time profile of high-order harmonic generation. In both cases, the population transfers which contribute to the generation of a particular set of harmonics occur at very specific times. In the usual three-step model, these times are such that the energy of a particular harmonic must be equal to the sum of the kinetic energy of the electron upon return and the atomic ionization potential. The same line of argumentation holds in the two-level case, but now the harmonic energy must be equal to the energy difference between the adiabatic states at these times.

Specifically for monochromatic driving fields, both models share several features. Both in the three-step model and in the two-level atom case there is a single time corresponding to the generation of the cutoff harmonic. In the former model, this time corresponds to the maximal kinetic energy the electron may have, upon return, whereas in the latter model it gives the maximal energy difference between the adiabatic states. Also for both cases, this time splits into two sets of times as the harmonic energy decreases. The interference between the corresponding population transfers originates the plateau in the high-order harmonic spectra. This pattern repeats itself every half cycle of the driving field. This is a direct consequence of the periodicity of the relevant physical quantities, namely the electron kinetic energy in the three-step model [33] and the adiabatic energies $\varepsilon_{\pm}^A$ in the two-level atom case. All these features are observed as peaks in the Gabor transform of the dipole acceleration. In the three-step model framework, analogous studies have been performed in [3].

TABLE IV. Field and two-level atom parameters, given in atomic units, together with the dilatation factor λ. All parameters have been chosen such that $\gamma_1=0.0391$ and $\gamma_2=0.3197$.

x_{10}	E_0	ω	ω_{10}	λ
1.066	0.6	0.05	0.409	1
9.535	8.385×10^{-4}	6.25×10^{-4}	5.1125×10^{-3}	1/80
47.673	6.71×10^{-6}	2.5×10^{-5}	2.045×10^{-4}	1/2000

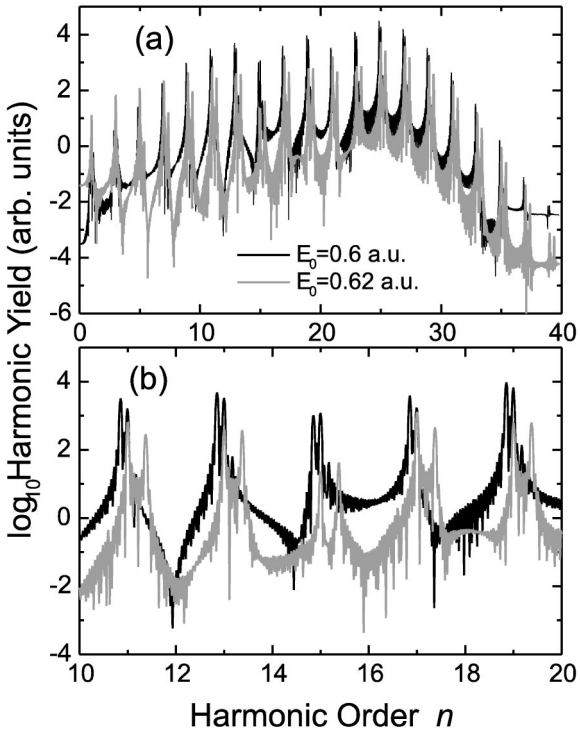

FIG. 15. Harmonic spectrum for the same parameters as in Fig. 4, compared to the one obtained for $E_0=0.62$ a.u., $\omega=0.05$ a.u., $\omega_{10}=0.409$ a.u., and $x_{10}=1.066$ a.u., respectively. These parameters give $\gamma_1=0.0378$, $\gamma_2=0.3094$, whereas the ones in Fig. 4 yield $\gamma_1=0.0391$, $\gamma_2=0.3197$. Part (a) shows the whole spectra, whereas part (b) displays both spectra for harmonic order $10<N<20$, such that their substructure can be seen. The field is switched on linearly within two cycles.

Also for bichromatic driving fields, there are several characteristics which are present in both models. A good example is the multiple cutoff structure. Indeed, the harmonic spectra in this case may exhibit several cutoffs, which, depending on the model in question, are given by the maxima of either the electron kinetic energy or of the energy difference between the adiabatic states. The number of these cutoffs, as well as their energies or the corresponding population-transfer times, are determined by the frequency ratio n, the field-strength ratio ζ, and the relative phase θ. For both the three-step model and the two-level atom, all peaks in the Gabor spectra can be traced back to the population-transfer times. In one or the other case, these population transfers occur either between the adiabatic states (Sec. IV), or between the ground-state and the continuum [8].

Similarities between the two models are also observed for the probability that the ''first step,'' i.e., population transfer, takes place. In the three-step model, this probability, per unit time, is roughly given by the quasi-static tunneling rate $\mathcal{P}\sim\exp[-\mathcal{C}/|E(t_0)|]$ [34]. A strong field $E(t_0)$ at the ionization time t_0 yields strong harmonics at the recombination time t_1. This relation is very useful for controlling harmonic spectra, as, for instance, the relative intensities of a double plateau (see, e.g., [8,9] for concrete examples). Within the two-level atom framework and in the monochromatic case, to first approximation, the field-dependent terms of the two-level Hamiltonian can be linearized at the crossings [14]. Thus the population transfer between the exchanged states can be computed by means of the Landau-Zener model [28,35]. This probability is approximately given by $\mathcal{P}\sim\exp[-\mathcal{C}'\pi/(2x_{10}E_0)]$, such that the Rabi frequency, in the two-level atom, plays a similar role as $E(t_0)$ in the three-step model. In general, however, there is not always a simple expression for the population transfer at a level crossing [28,31], such that $\mathcal{P}$ has to be computed according to the problem at hand. For instance, $\mathcal{P}$ may be rather complicated for bichromatic fields. This is a limitation for controlling high-order harmonic spectra in this latter case.

A particularity of the two-level atom is that the very same distortions caused by the additional field in the field-dressed energies, as functions of time, are also present in the adiabatic-state populations $|C_n^A(t)|^2$ and in the dipole acceleration. Specifically for the bichromatic field addressed in this paper, i.e., a $\omega-2\omega$ field, the whole pattern is no longer periodic in $T/2$, but in T. This is a consequence of the periodicity of the adiabatic states, which changes with the additional driving wave. A similar feature occurs in the three-step model framework, due to an analogous change in the electron kinetic energy upon return (see, e.g., [8,9] for a discussion of this issue).

An interesting issue which is not discussed in this paper concerns the influence of ionization or feedback mechanisms on the time profiles of harmonic generation by a two-level atom. In a previous paper it was shown that the main contributions to harmonic generation from a two-level atom whose states decayed according to quasi-static ionization rates occurred at minimal field. These results did not agree with the bound-bound transitions computed from the numerical solution of the Schrödinger equation for a Gaussian potential with two strongly coupled bound states [15]. The strikingly different time profiles obtained in the present paper for HHG in a closed two-level atom suggest, however, that these features are stongly influenced by ionization. Therefore more accurate descriptions of ionization and an adequate feedback mechanism from the continuum would be necessary in the two-level atom case with unstable levels. The influence of level widths on the population transfer between quantum states is discussed in [36].

Finally, there are scaling laws which allow extending the studies performed in this paper to a broader parameter range. In fact, we have shown that the important parameters for determining the physical behavior of the system are $\gamma_1=\omega/(2x_{10}E_0)$, and $\gamma_2=\omega_{10}/(2x_{10}E_0)$, which denote the ratio of the field and transition frequencies to the Rabi frequency, respectively. As long as γ_1 and γ_2 are kept constant, driving fields of completely different strengths and frequencies acting on systems of completely different energy gaps can yield similar spectra. For bichromatic fields, additional requirements for this invariance are fixed field-strength ratio ζ, field-frequency ratio n, and relative phase θ.

A concrete example of a system for which these properties may be applied is, for instance, a quantum well with $\omega_{10}\sim10^{-4}$ a.u., and $x_{10}\sim100$ a.u., subject to a field of strength $E_0\sim10^{-5}$ a.u. and frequency $\omega\sim10^{-5}$ a.u. [24]. Transitions between two subbands in these systems are de-

scribed very frequently by the semiconductor Bloch equations in the Hartree-Fock approximation [25]. In case collective effects can be neglected, the corresponding Hamiltonian reduces to a two-level one-particle Hamiltonian. In such a case, the results of the present paper are expected to be applicable.

Summarizing, we investigated the physical mechanism of HHG in a two-level atom for monochromatic and bichromatic driving fields, drawing a parallel between such a mechanism and the three-step model, and providing examples of how to control the resulting harmonic spectra. Such studies are motivated by the fact that, in order to understand HHG in more complex systems, one must first address the simplest case for which transitions involving bound states are important: a two-level atom. The present work is meant to be a contribution to a deeper understanding of HHG in this model, and a first step towards other systems where bound-bound transitions play a role. In fact, the three-step process discussed in this paper is expected to exist for more complex systems, which, in the presence of a periodic external field, exhibit several level crossings, analogous to those discussed here.

ACKNOWLEDGMENTS

We thank M. E. Madjet for beneficial discussions, A. Fring for useful comments on the manuscript, and S. W. Kim and T. Chakraborty for providing references.

[1] For a review on high-order harmonic generation, see, e.g., P. Salières, A. L'Huillier, Ph. Antoine, and M. Lewenstein, Adv. At., Mol., Opt. Phys. **41**, 83 (1999); T. Brabec and F. Krausz, Rev. Mod. Phys. **72**, 545 (2002).

[2] S.C. Rae, K. Burnett, and J. Cooper, Phys. Rev. A **50**, 3438 (1994); P. Antoine, B. Piraux, and A. Maquet, *ibid.* **51**, R1750 (1995); P. Antoine, B. Piraux, D.B. Milošević, and M. Gajda, *ibid.* **54**, R1761 (1996).

[3] P. Antoine, A. L'Huillier, and M. Lewenstein, Phys. Rev. Lett. **77**, 1234 (1996); C. Figueira de Morisson Faria, M. Dörr, and W. Sandner, Phys. Rev. A **55**, 3961 (1997); P. Antoine, B. Piraux, D.B. Milošević, and M. Gajda, Laser Phys. **7**, 594 (1997).

[4] See, e.g., B. Sundaram and P.W. Milonni, Phys. Rev. A **41**, 6571 (1990); L. Plaja and L. Roso-Franco, J. Opt. Soc. Am. B **9**, 2210 (1992); A.E. Kaplan and P.L. Shkolnikov, Phys. Rev. A **49**, 1275 (1994); S. de Luca and E. Fiordilino, J. Phys. B **29**, 3277 (1996).

[5] M.Yu. Kuchiev, Pis'ma Zh. Éksp. Teor. Fiz. **45**, 319 (1987) [JETP Lett. **45**, 404 (1987)]; P.B. Corkum, Phys. Rev. Lett. **71**, 1994 (1993); K. C. Kulander, K. J. Schafer, and J. L. Krause, in *Proceedings of the SILAP Conference*, edited by B. Piraux *et al.* (Plenum, New York, 1993); M. Lewenstein, Ph. Balcou, M.Yu. Ivanov, A. L'Huillier, and P.B. Corkum, Phys. Rev. A **49**, 2117 (1994); W. Becker, S. Long, and J.K. McIver, *ibid.* **41**, 4112 (1990); **50**, 1540 (1994).

[6] See, e.g., M. Bellini, C. Lynga, A. Tozzi, M.B. Gaarde, T.W. Hänsch, A. L'Huillier, and C.-G. Wahlström, Phys. Rev. Lett. **81**, 297 (1998); M.B. Gaarde, F. Salin, E. Constant, Ph. Balcou, K.J. Schafer, K.C. Kulander, and A. L'Huillier, Phys. Rev. A **59**, 1367 (1999); P. Balcou, A.S. Dederichs, M.B. Gaarde, and A. L'Huillier, J. Phys. B **32**, 2973 (1999).

[7] See, e.g., D.B. Milošević, W. Becker, and R. Kopold, Phys. Rev. A **61**, 063403 (2000); D.B. Milošević and W. Becker, *ibid.* **62**, 011403 (2000); C. Figueira de Morisson Faria, D.B. Milošević, and G.G. Paulus, *ibid.* **61**, 063415 (2000); C. Figueira de Morisson Faria and M.L. Du, *ibid.* **64**, 023415 (2001), and references therein.

[8] C.F. de Morisson Faria, M. Dörr, W. Becker, and W. Sandner, Phys. Rev. A **60**, 1377 (1999).

[9] C. Figueira de Morisson Faria, W. Becker, M. Dörr, and W. Sandner, Laser Phys. **9**, 388 (1999).

[10] M.Q. Bao and A.F. Starace, Phys. Rev. A **53**, R3723 (1993); A. Lohr, W. Becker, and M. Kleber, Laser Phys. **7**, 615 (1997); B. Wang, X. Li, and P. Fu, J. Phys. B **31**, 1961 (1998); D.B. Milošević and A.F. Starace, Phys. Rev. A **60**, 3160 (1999); Phys. Rev. Lett. **82**, 2653 (1999); Laser Phys. **10**, 278 (2000).

[11] A. de Bohan, Ph. Antoine, D.B. Milošević, and B. Piraux, Phys. Rev. Lett. **81**, 1837 (1998); A. de Bohan, Ph. Antoine, D.B. Milošević, G.L. Kamta, and B. Piraux, Laser Phys. **9**, 175 (1999).

[12] C. Figueira de Morisson Faria and J.M. Rost, Phys. Rev. A **62**, 051402(R) (2000).

[13] See, e.g., M.D. Perry and J.K. Crane, Phys. Rev. A **48**, R4051 (1993); H. Eichmann, S. Meyer, K. Riepl, C. Momma, and B. Wellegehausen, *ibid.* **50**, R2834 (1994); S. Watanabe, K. Kondo, Y. Nabekawa, A. Sagisaka, and Y. Kobayashi, Phys. Rev. Lett. **73**, 2692 (1994); M. Ivanov, P.B. Corkum, T. Zuo, and A. Bandrauk, *ibid.* **74**, 2933 (1994); H. Eichmann, A. Egbert, S. Nolte, C. Momma, B. Wellegehausen, W. Becker, S. Long, and J.K. McIver, Phys. Rev. A **51**, R3414 (1995); M.B. Gaarde, P. Antoine, A. Persson, B. Carré, A. L'Huillier, and C.-G. Wahlström, J. Phys. B **29**, L163 (1996).

[14] F.I. Gauthey, B.M. Garraway, and P.L. Knight, Phys. Rev. A **56**, 3093 (1997).

[15] C. Figueira de Morisson Faria, M. Dörr, and W. Sandner, Phys. Rev. A **58**, 2990 (1998).

[16] For the first experimental evidence of materials that can survive intensities of the order of 10^{14} W/cm^2, consult M. Lenzner, J. Krüger, S. Sartania, Z. Cheng, Ch. Spielmann, G. Mourou, W. Kautek, and F. Krausz, Phys. Rev. Lett. **80**, 4076 (1998).

[17] O.E. Alon, V. Averbukh, and N. Moiseyev, Phys. Rev. Lett. **80**, 3743 (1998); K. Z. Hatsagortsyan and C. H. Keitel, *ibid.* **86**, 12277 (2001); J. Phys. B **35**, L175 (2002).

[18] O.E. Alon, V. Averbukh, and N. Moiseyev, Phys. Rev. Lett. **85**, 5218 (2000); G.Ya. Slepyan, S.A. Maksimenko, V.P. Kalosha, A.V. Gusakov, and J. Herrmann, Phys. Rev. A **63**, 053808 (2001).

[19] This phenomenon has been observed experimentally for extremely short pulses ($5fs$) and peak intensities of 10^{12} W/cm^2 in O.D. Mücke, T. Tritschler, M. Wegener, U. Morgner, and F.X. Kärtner, Phys. Rev. Lett. **87**, 057401 (2001).

[20] M. Yu Ivanov, P. Hawrylak, P. Haljan, T. Fortier, and P. B. Corkum (unpublished).

[21] See, e.g., N. Hay, M. Castillejo, R. de Nalda, E. Springate, K.J. Mendham, and J.P. Marangos, Phys. Rev. A **61**, 053810 (2000); N. Hay, R. de Nalda, T. Halfmann, K.J. Mendham, M.B. Mason, M. Castillejo, and J.P. Marangos, *ibid.* **62**, 041803 (2000).

[22] V. Averbukh, O.E. Alon, and N. Moiseyev, Phys. Rev. A **64**, 033411 (2001).

[23] W. Chism, T. Timberlake, and L.E. Reichl, Phys. Rev. E **58**, 1713 (1998); T. Timberlake and L.E. Reichl, Phys. Rev. A **59**, 2886 (1999); Phys. Rev. A **64**, 033404 (2001).

[24] See, e. g., B. Birnir, B. Galdrikian, R. Grauer, and M. Sherwin, Phys. Rev. B **47**, 6795(R) (1993).

[25] D.E. Nikonov, A. Imamoğlu, L.V. Butov, and H. Schmidt, Phys. Rev. Lett. **79**, 4633 (1997); J.L. Krause, D.H. Reitze, G.D. Sanders, A.V. Kuznetsov, and C.J. Stanton, Phys. Rev. B **57**, 9024 (1998).

[26] See, e.g., J.N. Heyman, K. Craig, B. Galdrikian, M.S. Sherwin, K. Campman, P.F. Hopkins, S. Fafard, and A.C. Gossard, Phys. Rev. Lett. **72**, 2183 (1994); B. Galdrikian, and B. Birnir, *ibid.* **76**, 3308 (1996).

[27] L. Allen and J. Eberly, *Optical Resonance and Two-Level Atoms* (Wiley, New York, 1975).

[28] For a discussion of the existing analytical solutions for several types of level crossings and of the transformation to the adiabatic basis, see, e.g., K.-A. Suominen and B.M. Garraway, Phys. Rev. A **45**, 374 (1992).

[29] These structures have been investigated in B.M. Garraway and N.V. Vitanov, Phys. Rev. A **55**, 4418 (1997) within a different context.

[30] Hyper-Raman lines appear in the spectra at frequencies different from the harmonics. For a detailed discussion of these lines see, e.g., F.I. Gauthey, C.H. Keitel, P.L. Knight, and A. Maquet, Phys. Rev. A **52**, 525 (1995); M.L. Pons, R. Taieb, and A. Maquet, *ibid.* **54**, 3634 (1996); A. Di Piazza, E. Fiordilino, and M.H. Mittleman, *ibid.* **64**, 013414 (2001).

[31] K.-A. Suominen, B.M. Garraway, and S. Stenholm, Opt. Commun. **82**, 260 (1991); K.-A. Suominen, *ibid.* **93**, 126 (1992); N.V. Vitanov and B.M. Garraway, Phys. Rev. A **53**, 4288 (1996); N.V. Vitanov, *ibid.* **59**, 988 (1999).

[32] C. Figueira de Morisson Faria, A. Fring, and R. Schrader, J. Phys. B **33**, 1675 (2000).

[33] The kinetic energy in this case is given by $E_{\mathrm{kin}}(t_1,t_0)=1/2[A(t_1)-A(t_0)]^2$, where $A(t)$ is the vector potential. Clearly, if $A(t+\pi/\omega)=\pm A(t)$, which is the case for monochromatic and bichromatic fields with odd frequency ratios, $E_{\mathrm{kin}}(t_0,t_1)=E_{\mathrm{kin}}(t_0+\pi/\omega,t_1+\pi/\omega)$.

[34] See, e.g., L. D. Landau and E. M. Lifshitz, *Quantum Mechanics* (Pergamon, Oxford, 1977).

[35] L.D. Landau, Phys. Z. Sowjetunion **2**, 46 (1932); C. Zener, Proc. R. Soc. London, Ser. A **137**, 696 (1932).

[36] C.A. Moyer, Phys. Rev. A **64**, 033406 (2001).